The Astrophysical Journal, 849:147 (8pp), 2017 November 10 https://doi.org/10.3847/1538-4357/aa901d

Disentangling the Radio Emission of the Supernova Remnant W51C

M. F. Zhang[1,2], W. W. Tian[1,2,3], D. A. Leahy[3], H. Zhu[1,4], X. H. Cui[1], and S. S. Shan[1,2]
[1] Key Laboratory of Optical Astronomy, National Astronomical Observatories, Chinese Academy of Sciences, Beijing 100012, China; tww@bao.ac.cn
[2] University of Chinese Academy of Sciences, 19A Yuquan Road, Shijingshan District, Beijing 100049, China
[3] Department of Physics & Astronomy, University of Calgary, Calgary, Alberta T2N 1N4, Canada
[4] Harvard-Smithsonian Center for Astrophysics, 60 Garden Street, Cambridge, MA 02138, USA
Received 2017 August 10; revised 2017 September 19; accepted 2017 September 27; published 2017 November 9

Abstract

We simulate the evolution of supernova remnant (SNR) W51C. The simulation shows the existence of a new northeast edge. We present the magnetic field structure of the W51 complex (SNR W51C and two H II regions W51A/B) by employing the 11 cm survey data of Effelsberg. This new edge is identified and overlaps with W51A along the line of sight, which gives a new angular diameter of about 37′ for the quasi-circular remnant. In addition, we assemble the OH spectral lines (1612/1665/1720 MHz) toward the complex by employing the newly released *THOR* (The HI OH Recombination line survey of Milky Way) data. We find that the known 1720 MHz OH maser in the W51B/C overlap area is located away from the detected 1612/1665 MHz absorption region. The latter is sitting at the peak of the H II region G49.2-0.35 within W51B.

Key words: ISM: individual objects (W51 A/B/C) – ISM: magnetic fields – magnetohydrodynamics (MHD) – masers

1. Introduction

The interaction between supernova remnants (SNRs) and molecular clouds (MCs) has an impact on star formation, the origin of cosmic rays, and the Galactic interstellar medium (ISM). The shocks of supernovae can compress MCs, and could be a good catalyst for star formation. The shock can also dissociate molecules and generate high-energy particles, which are an important source of Galactic cosmic rays. Most of the heavy elements are produced through supernova explosions, while the interaction between SNR shocks and MCs plays a key role in the synthesis of various ISM molecules. A detailed study on SNR–MC interaction can helpus understand these physical processes better.

The W51 complex is composed of two H II regions (W51A/B) and one SNR (W51C). Both H II regions are extended and consist of many small H II structures, such as G49.2-0.35. W51C has a thick semicircular shell of 14′ × 20′ (Copetti & Schmidt 1991; Subrahmanyan & Goss 1995) in the radio continuum image, one side of which adjoins the H II region W51B. Recent observations show high-energy features in the boundary (Abdo et al. 2009; Aleksić et al. 2012), which are regarded as strong evidence of interaction between the SNR and MCs. In the east of W51B, i.e., next to the SNR explosion center, 1720 MHz OH masers were discovered (Hewitt et al. 2008; Brogan et al. 2013), which is further evidence supporting an interaction. The W51A is an active star formation region, but does not show any sign of connection with W51C. W51A and W51B are connected along the line of sight (LoS) in CO and infrared images (Kang et al. 2010; Parsons et al. 2012; Ginsburg et al. 2015). They have distances of 5 kpc ∼ 8 kpc (Genzel et al. 1981; Schneps et al. 1981; Xu et al. 2009; Sato et al. 2010; Tian & Leahy 2013). For comparison, the distance of SNR W51C is 4.3 kpc (Tian & Leahy 2013) to 6 kpc (Koo et al. 1995). The spatial location of the three sources seems to hint at a physical connection among them.

Many observations of the complex have been done so far, but the physical association among the major structures of the complex is still not clear. Thus, we create an MHD simulation of the SNR in order to study the possible physical connection between the remnant and the H II regions. In addition, we analyze the polarization data and the OH spectra data to understand the simulation results.

In Section 2, we describe the data and processing method. In Section 3, we give the simulation model and list the parameters we use. In Section 4, we present the results. In Section 5, we discuss the results. Section 6 is a summary.

2. Data Reduction

The data used for generating the magnetic field structure is from the Effelsberg 11 cm (2.695 GHz) survey[5] (Duncan et al. 1999). Duncan et al. (1999) presented a polarization map covering the W51 region. They smoothed the map to cover a larger region, which obscured some small structures. The resolution of the original 11 cm data is 5′ and the resolution of the smoothed images is 12′. In Figure 5, we show the map of W51 at 5′ resolution and rotate the polarization direction 90° to get an estimate of the magnetic direction, i.e., the arrows indicate magnetic direction, while the arrow length indicates polarization intensity. Because the 11 cm data have an instrumental polarization of 0.7% ± 0.25% (Junkes et al. 1987), we have to subtract the instrumental polarization intensity. At first, we delete the part of the data with values below one standard deviation in the total intensity image. Then we obtain the polarization intensity by $I_{\rm pol}^{\rm final} = I_{\rm pol}^{\rm primary} - I_{\rm total} * 0.007$ and set negative values to zero. Here $I_{\rm pol}^{\rm final}$ is the obtained polarization intensity, $I_{\rm pol}^{\rm primary}$ is the original polarization intensity, and $I_{\rm total}$ is the total continuum intensity. Finally, we obtain the degree of polarization by $p = I_{\rm pol}^{\rm final}/I_{\rm total}$. In fact, the instrumental polarization intensity in part of the area may be less than 0.7%, so our subtracted map shows many negative values. In our processing, all negative values are set to zero. The continuum and polarization sensitivity of the survey are 20 mK and 11 mK respectively.

[5] http://www3.mpifr-bonn.mpg.de/survey.html

We use the newly released data from *THOR* DR1 (Beuther et al. 2016). DR1 consists of the 1.4 GHz continuum maps, HI, OH spectral line maps (1612/1665/1720 MHz) and radio recombination line maps, covering a region with $15^\circ < l < 67^\circ$, $-1^\circ < b < 1^\circ$. The spatial resolution of the OH spectral lines is about $20''$ and the velocity resolution is about 1.5 km s^{-1}. Because the OH maser lines are so strong that we cannot plot them with other spectral lines at the same scale, we modify the spectral scale in maser regions, where the spectral intensities are divided by 20.

The 1.4 GHz continuum image is from the *VGPS* (VLA Galactic Plane Survey; Stil et al. 2006). The spatial resolution of the *VGPS* is $1'$ and the sensitivity is 2 K.

3. Simulation Model

The simulation is based on a three-dimensional MHD (magnetohydrodynamic) model in which we ignore all dissipative effects, such as viscosity, resistivity, and thermal conduction. Gravitation and radiation cooling are also removed from the model, because they have little influence on the simulation.

In terms of MHD theory, the ideal conservation equation is

$$\begin{cases} \dfrac{\partial \rho}{\partial t} + \nabla \cdot (\rho \boldsymbol{v}) = 0, \\ \dfrac{\partial \rho \boldsymbol{v}}{\partial t} + \nabla \cdot (\rho \boldsymbol{v}\boldsymbol{v} - \boldsymbol{B}\boldsymbol{B}) + \nabla P^* = 0, \\ \dfrac{\partial E}{\partial t} + \nabla \cdot [(E + P^*)\boldsymbol{v} - \boldsymbol{B}(\boldsymbol{v} \cdot \boldsymbol{B})] = 0, \\ \dfrac{\partial \boldsymbol{B}}{\partial t} + \nabla \times (\boldsymbol{v} \times \boldsymbol{B}) = 0, \end{cases} \quad (1)$$

in which, ρ is mass density, $\boldsymbol{v}$ is velocity, $\boldsymbol{B}$ is magnetic field intensity, P^* is total pressure, and E is total energy density.

Sasaki et al. (2014) estimated W51C's progenitor mass to be more than 20 $M_\odot$ using a distance of 6 kpc. This distance is an upper limit, so the real mass is less. In the simulation, we use 20 $M_\odot$ as the progenitor mass, then the ejecta mass should be 11 $M_\odot$ (Sukhbold et al. 2016). Koo et al. (1995) estimated an explosion energy of 3.6×10^{51} erg s^{-1}, which is larger than the canonical value, $1 \sim 3 \times 10^{51}$ erg s^{-1} (Poznanski 2013). For W51C, the explosion energy should be about 1.0×10^{51} erg s^{-1} based on the work of Poznanski (2013). Although Poznanski (2013) only estimated the kinetic energy of SNRs, those SNRs are so young that we think the kinetic energy is nearly equal to the total explosion energy. In contrast, W51C is a middle-aged SNR, thus its initial explosion energy is the sum of the present kinetic energy and thermal energy. Using a distance of 6 kpc, Koo et al. (1995) derived the thermal energy and estimated the explosion energy according to Sedov model (Sedov 1959). Taking the recent measured distance of 4.3 kpc (Tian & Leahy 2013), we employ the same method as Koo et al. (1995) and get an explosion energy of 1.3×10^{51} erg s^{-1}, more reasonable for such a progenitor and similar to the estimation based on the work of Poznanski (2013). Of course, the explosion energies of SNRs vary in a large range (Leahy 2017), so it cannot be used to determine which distance is right. 4.3 kpc is more reliable in terms of present evidences, so we use it as the distance of W51C. We take the region of $48.^\circ89 < l < 49.^\circ51$, $-0.^\circ81 < b < -0.^\circ19$ as the new size of W51C. For such a quasi-circular SNR with an angular diameter of about $37'$, its shock diameter is 46 pc. The age is 18,000 years, if we use the shock velocity 490 km s^{-1} derived by Koo et al. (1995).

We use a python calculator for simulating SNR evolution (Leahy & Williams 2017) to estimate the ambient density of 0.21 cm^{-3}. To simulate a random distribution of density, we adopt a power-law density distribution $N(\rho) = N_0 \rho^{-\alpha}$, in which $N(\rho)$ is the pixel numbers at different densities, N_0 is a constant, α is the power-law index, which is a positive number, i.e., low-density regions are larger than high-density regions. For example, there are $256 \times 256 \times 256$ pixels in our simulation, then there are possibly 10,000,000 pixels with densities lower than 0.21 cm^{-3} and only 100 pixels with densities higher than 21 cm^{-3}. In the initial conditions, we only warrant the mean density of 0.21 cm^{-3}. Parsons et al. (2012) studied the molecular clumps (including dense clumps) and found that their mass distribution follows a power law with an index of 2.4, which may imply the distribution of ambient density. For this region, no atomic hydrogen density distribution is given at present, so we take $\alpha = 2.4$ in the initial density distribution. In addition, to simulate the interaction, we add an MC with a density of 2 cm^{-3} and a diameter of 11 pc (see the two middle panels of Figure 1).

For the magnetic field, we apply a direction of 45° rotating anti-clockwise from the Galactic plane to reconstruct the morphology of W51C to match the direction of W51C edge. We assume that the magnetic direction is the same in this region. We want to reproduce a much lower radio surface brightness for the upper rim of W51C compared to the lower rim because we want to derive the largest difference between the new edge and the old edge of W51C, so that we can get the smallest radio flux density of the new edge. Meanwhile, the magnetic intensity should be reasonable. The reasonable magnetic intensity in the Milky Way is from 4 to 14 μG (Haverkorn 2015). The length range in the simulation is $75 \times \sqrt{2}$ pc. Then the magnetic gradient is 0.1 μG pc^{-1} and the central magnetic field is 9 μG.

In the simulation, a region of $1^\circ \times 1^\circ$ is 75 pc × 75 pc in real space. For such a region, we generate a grid of $256 \times 256 \times 256$, i.e., its resolution is 0.3 pc pixel^{-1} ($0.'24$ pixel^{-1}). To get an approximate circular explosion and ensure the shock is still in an ejecta-dominated phase at initial time, we use 4 pc as the initial radius. For SNR W51C, it would take about 850 years to expand to 4 pc in size. Meanwhile, the Sedov time of SNR W51C is 3200 years (Leahy & Williams 2017), so it is before the Sedov phase and the setting is appropriate. In Figure 1, the top panels show the initial conditions in the simulation.

To compare with real observations, we use $i(\nu) = C\rho B_\perp^{\beta+1}\nu^{-\beta}$ (Orlando et al. 2007) to get the relative radio flux volume density, in which ν is the radiation frequency, C is a constant, ρ is the density, $B_\perp$ is the magnetic field perpendicular to the LoS and β is the synchrotron spectral index. By employing $\int i(\nu)dl$, we integrate $i(\nu)$ along LoS to obtain relative radio flux density. In this simulation, the x-axis is defined as the direction of LoS. We assume all radio radiation originates from a synchrotron mechanism. For the interaction region, we think that about 10% of the material contributes to the radio flux density, i.e., $i(\nu) = 0.1C\rho B_\perp^{\beta+1}\nu^{-\beta}$. The ρ and $B_\perp$ are derived by simulation, while the β is 0.25 for W51C

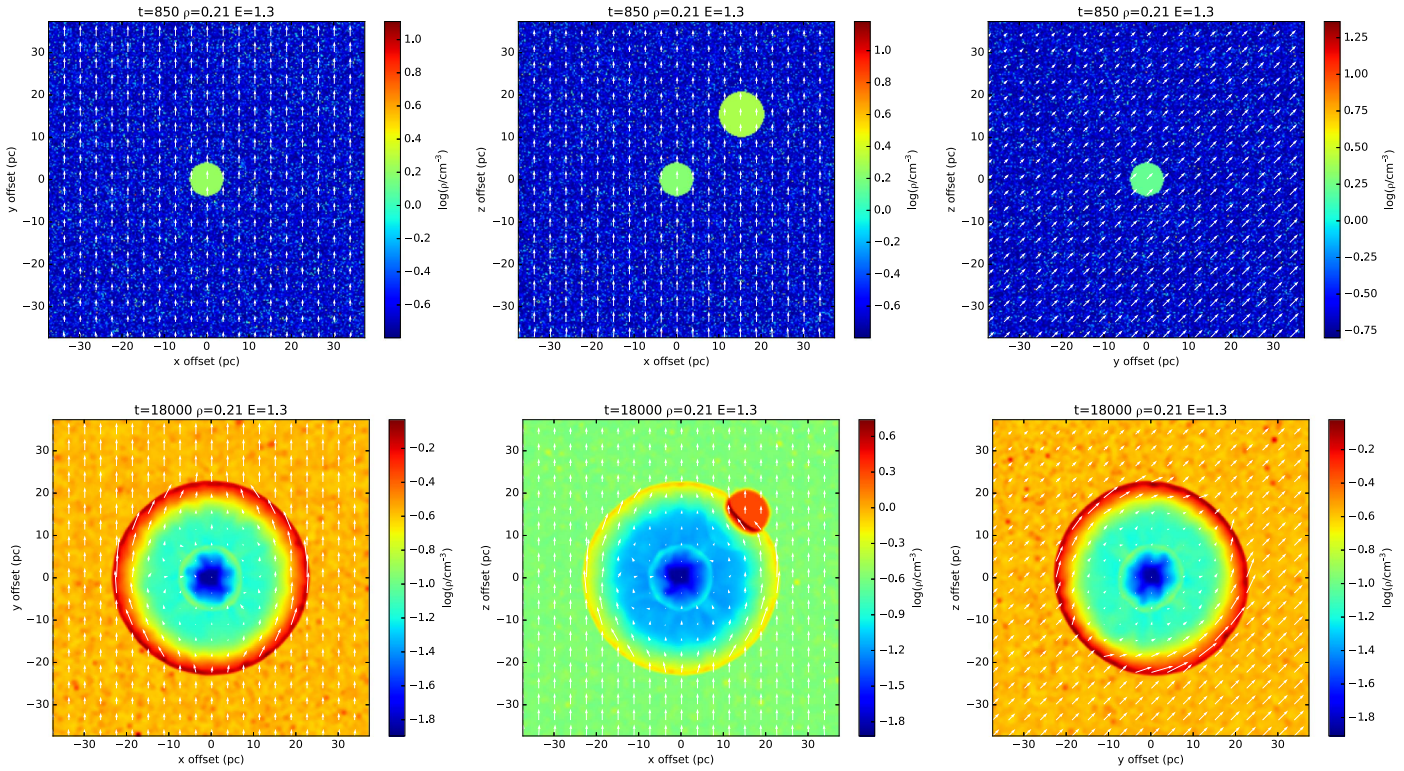

Figure 1. Simulated density–magnetic field images. The images are slices through the center of the box along each axis. The background is the density distribution, while the white arrows show the direction and intensity of the magnetic field. The top panels show the initial conditions in the simulation, while the bottom panels show the result after 18,000 years. The central magnetic intensity is 9 μG in the top panels.

(Shaver & Goss 1970). Then we get a radio image. The resolution of the *VGPS* continuum image is $1'$ and the full width at half maximum (FWHM) for a Gaussian function is $2\sqrt{2\ln 2}\,\sigma$, in which the Gaussian function is

$$G(x) = \frac{1}{\sigma\sqrt{2\pi}} e^{-\frac{1}{2}\left(\frac{x-\mu}{\sigma}\right)^2}, \quad (2)$$

where σ is the standard deviation and μ is the expectation value. The resolution is equal to the FWHM, so the $\sigma = 0\farcm42$ for a beam of *VGPS*. In our simulation, the resolution is $0\farcm12\,\mathrm{pixel}^{-1}$, so the $\sigma = 3.5$ referring to the number of pixels. For simplicity, we set $\sigma = 4$. Thus, we smooth the image using a 2D Gaussian function with $\sigma = 4$.

The evolutions with different parameters are included in the work. We take 2.0 and 3.0×10^{51} erg as possible explosion kinetic energy for W51C, while we keep other parameters the same as the previous settings. We also, respectively, set $0.13\,\mathrm{cm}^{-3}$ and $0.3\,\mathrm{cm}^{-3}$ as the mean ISM density of the whole region.

We use PLUTO[6] (Mignone et al. 2007) to perform the simulation. The initial conditions are summarized in Table 1, in which the parameters without references are from our estimations. According to our model, we simulate the evolution of SNR W51C until 18,000 years.

Table 1
Summary of Simulation Parameters on W51C

Parameters	Value	References
Ejecta Mass	11 $M_\odot$	1, 2
Initial Explosion Energy	1.3×10^{51} erg	3, 4
Initial Radius	4 pc	
Initial Time	850 years	5
Mean Density	$0.21\,\mathrm{cm}^{-3}$	4, 5
Density Index (α)	2.4	6
Magnetic Field Gradient	0.1 μG pc^{-1}	
Central Magnetic Intensity	9 μG	
Mean Atomic Weight	1.3	
Adiabatic Coefficient	5/3	
Temperature	100 K	
Synchrotron Index (β)	0.25	7
Distance	4.3 kpc	8

References. (1) Sasaki et al. (2014); (2) Sukhbold et al. (2016); (3) Poznanski (2013); (4) Koo et al. (1995); (5) Leahy & Williams (2017); (6) Parsons et al. (2012); (7) Shaver & Goss (1970); (8) Tian & Leahy (2013).

4. Results

4.1. Simulation

We present the simulation result at 18,000 years in the bottom panels of Figure 1. In the figure, the direction and length of arrows show the direction of magnetic field and the magnetic intensity, while the backgrounds show the density. We can see obvious magnetic amplification both at the shock region and the interaction region. In the y–$z$plane, the magnetic intensities on the UL (upper left) and LR (lower right) are larger than their surrounding regions, and the intensity of the LR is larger than that of the UL. The direction of the magnetic field follows the shapes of edges well. The density and magnetic intensity in the inner SNR become very low, while the outer shell is dense and has a stronger magnetic field.

[6] http://plutocode.ph.unito.it/

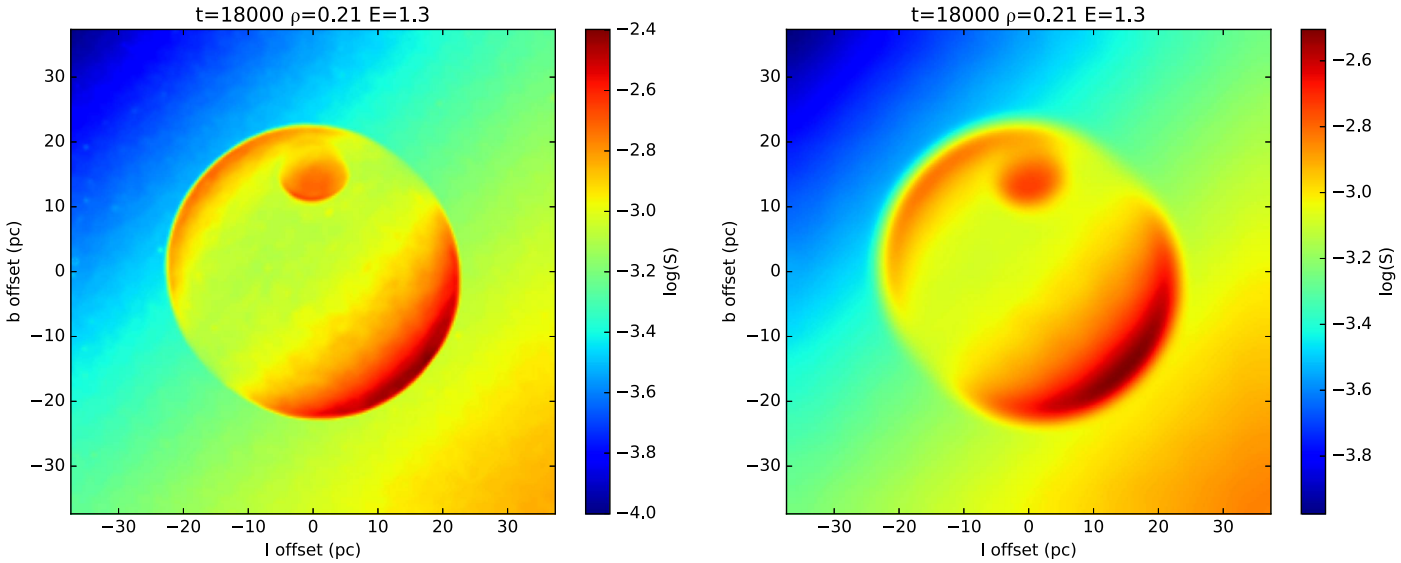

Figure 2. Relative radio flux density after 18,000 years for SNR W51C. The right panel results from Gaussian smoothing with $\sigma = 4$. Here, 1 pc is equal to $0\farcm8$ assuming a distance of 4.3 kpc.

Figure 2 shows the final radio flux density maps converted from the density maps. We test the simulation taking index = 1.0, 3.0. When taking index = 3.0, the radio image is similar to the image in Figure 2 at index = 2.4. When taking index = 1.0, the radio image shows more random components, but other features are similar to the image at index = 2.4. Thus we only present the results for index = 2.4.

The right panel uses $\sigma = 4$ for 2D Gaussian smoothing. The UL edge is weaker but still obvious. The center is the weakest region in the flux density image, and there is obvious radio emission toward the interaction region. Without the Gaussian smoothing, the simulation cannot produce the thickness of the real LR edge, even if we take the density distribution into consideration. However, when $\sigma = 4$, the simulation is consistent with the observation. Figure 3 shows that the UL edge is about two times dimmer than the LR edge.

The results based on different parameters are shown in Figure 4. The UL edge is obvious in all images.

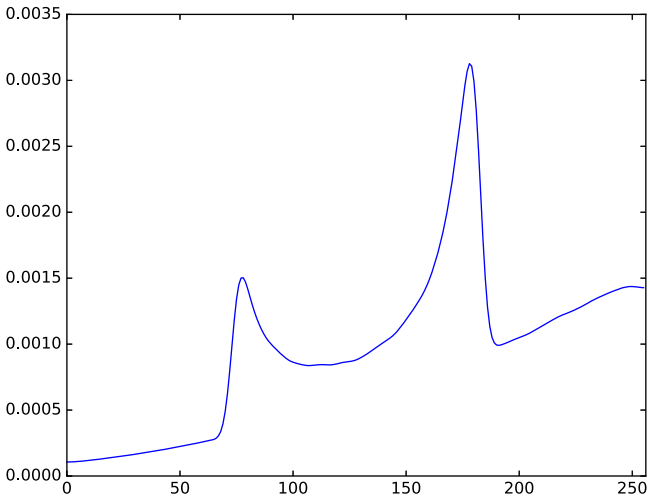

Figure 3. Relative radio flux density along the diagonal line of UL to LR in the right panel of Figure 2.

4.2. Magnetic Field

The observed magnetic field structure of W51C is shown in Figure 5. There are four regions with strong polarization, the northeast (NE), the middle (M), the northwest (NW), and the south (S). They all have similar magnetic field directions, even though the direction in the NE region is a little chaotic. The polarization of the NE region is the strongest. After subtracting the instrumental polarization, the polarization in the NW region disappears, while the other three regions still have polarization. The direction in the NE region becomes more regular, which possibly means we have subtracted enough instrumental polarization. The NE, M, and S regions, respectively, overlap with W51A, G49.2-0.35, and W51C well.

4.3. OH Masers and Absorption

There is a high-resolution 1720 MHz observation for the region (Brogan 2005), but no high-resolution 1665/1612 MHz observation. The *THOR* data make it possible to reveal the spatial relation between the 1720 MHz emission and the 1720/1665/1612 MHz absorption. We present OH spectral maps for the region in Figure 6. The background is the *THOR* 1.4 GHz continuum image. The 1720 MHz OH maser is strong and located away from the small H II region G49.2-0.35 in W51B. Here we want to indicate that the radio emission of the interaction region in our simulation, is totally different from H II region G49.2-0.35. In fact, we do not detect the radio emission from the interaction region, but the 1720 MHz OH maser and weak polarized radio emission are good evidence that it exists. The 1720/1665/1612 MHz OH absorption lines are obvious at the bright region of G49.2-0.35; however, at the dimmer region, there are some broader emission lines, in which the 1665 MHz OH emission is stronger. Meanwhile, some emission and absorption features are far away from the H II region. All the features have similar velocities, so they all possibly originate from the W51 complex.

Figure 7 shows the sites and the spectra of the H II region G49.2-0.35 and the 1720 MHz OH maser. In the top panel, the background is the *THOR* 1720 MHz channel map at 70.5 km s^{-1}, the contours show *THOR* 1.4 GHz continuum intensities. The bottom panel presents the spectra of the maser

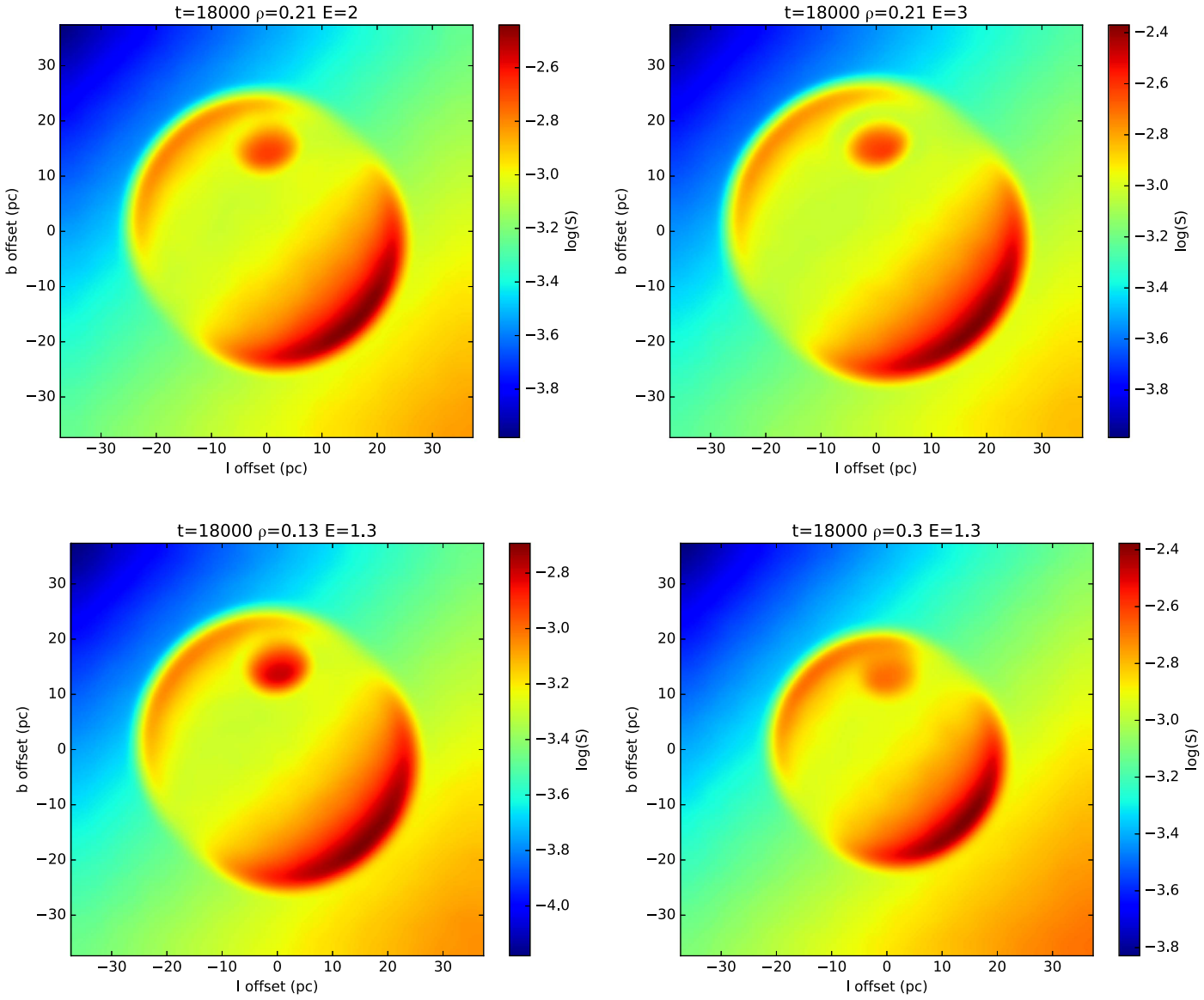

Figure 4. Relative radio flux density in different parameters with $\sigma = 4$. The top two panels change the explosion kinetic energy to 2.0 and 3.0 $\times$ 10^{51} erg, while the bottom two panels change the density of ISM to 0.13 cm^{-3} and 0.3 cm^{-3}. Here 1 pc is equal to $0'.8$ assuming a distance of 4.3 kpc.

region and H II region at different frequencies. The 1720 MHz OH maser is completely separated from the small H II region G49.2-0.35, but still in the large H II region W51B. The 1720 MHz peak and the 1720 MHz absorption feature have a velocity difference of 2 $\sim$ 3 km s^{-1}, the absorption velocities decrease with the decrease of frequencies.

5. Discussion

5.1. The New Northeast Edge

To get the semicircular shape, we modify the method used by Orlando et al. (2007). We find that the thickness of the shell is related to the density distribution of the ISM. In a uniform ISM, the shell is usually thinner (Orlando et al. 2007). We choose power-law distribution as the initial density distribution. Our simulation always shows that there appears to be a northeast edge at the site of W51A. Because the W51A is so bright that it totally covers the new edge, nobody in previous studies recognized such an edge (see the comparison between the observation image and the simulation image in Figure 8).

Based on the simulation result, the new edge is about two times dimmer than the southern edge (see Figure 3).

Combining the derivation and some observations, we can predict the flux density of the new edge. The southwestern edge of W51C has a brightness temperature of about 60 K at 1.4 GHz (see Figure 5), so the new northeastern edge should have a brightness temperature of 30 K, larger than the sensitivity of *VGPS*. Using a spectral index of 0.25, for W51C, we can get the brightness temperature of 14 K at 11 cm, then the new edge should have a brightness temperature of 7 K at 11 cm. The degree of polarization of W51C is $3^{+1.8}_{-1.0}\%$ (Velusamy & Kundu 1974) at 11 cm. If we believe that the degree of polarization of the new edge is the same as the detected edge, its polarization intensity should be approximately 210 mK, larger than the sensitivity of Effelsberg 11 cm polarization survey. The magnetic amplification in our simulation is obvious in the NE region, so its polarization flux density should be large. Generally, the polarization of an H II region at this wavelength is rare. If we find polarized light

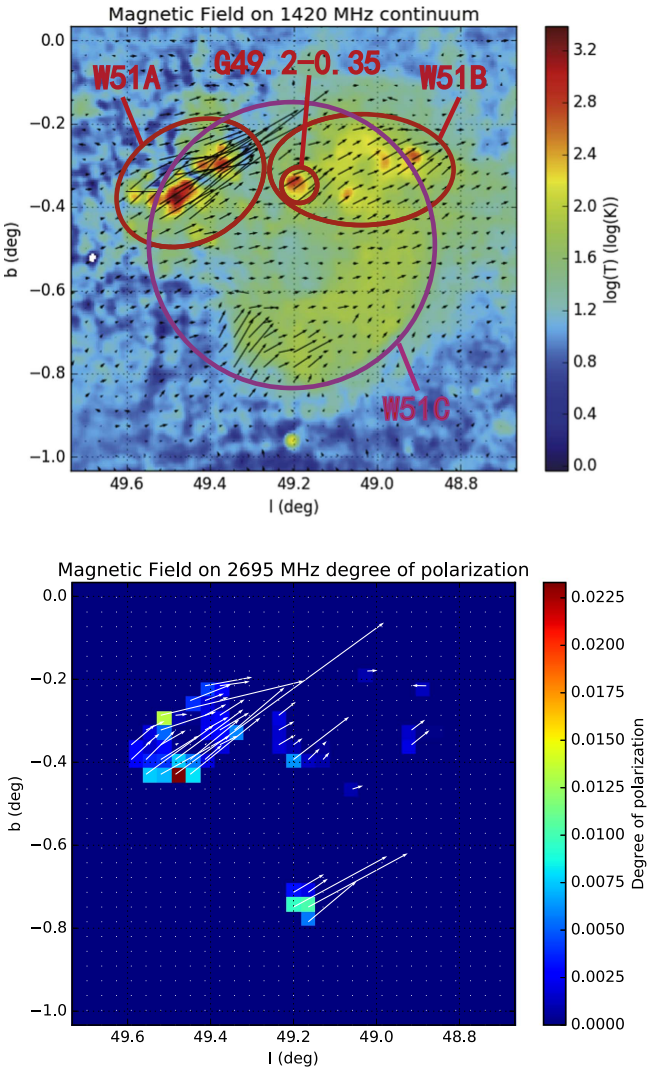

Figure 5. In the top panel, the background is a 1.4 GHz continuum image from *VGPS*, while the black arrows show the direction of the magnetic field. The length of arrows shows the polarization intensity (mK) and the largest intensity is 1581 mK. In the bottom panel, the background is the degree of polarization on 2695 MHz, while the white arrows show the direction of magnetic field. The length of arrows shows the degree of polarization and the largest degree of polarization is about 2%.

along the LoS of the NE region, it should originate from W51C not W51A.

Figure 5 truly reveals the polarized light toward the NE region. A part of SNR W51C, i.e., the southwestern region, in which Velusamy & Kundu (1974) discovered obvious polarization, does not show any polarization in Figure 5. This is possibly because we subtract too much instrumental polarization, which implies the polarization in the present image is possibly the lower limit. The NE and S regions have same magnetic field direction, which is similar to our simulation. Since the polarized emission of the S region is from W51C, the polarization of the NE region is likely also from W51C. The directions of instrumental polarization (Junkes et al. 1987) and background polarization (Duncan et al. 1999) are both different from the direction of observed polarization in this region. Moreover, there is no other polarized source toward this region (Xu & Han 2014). Thus,

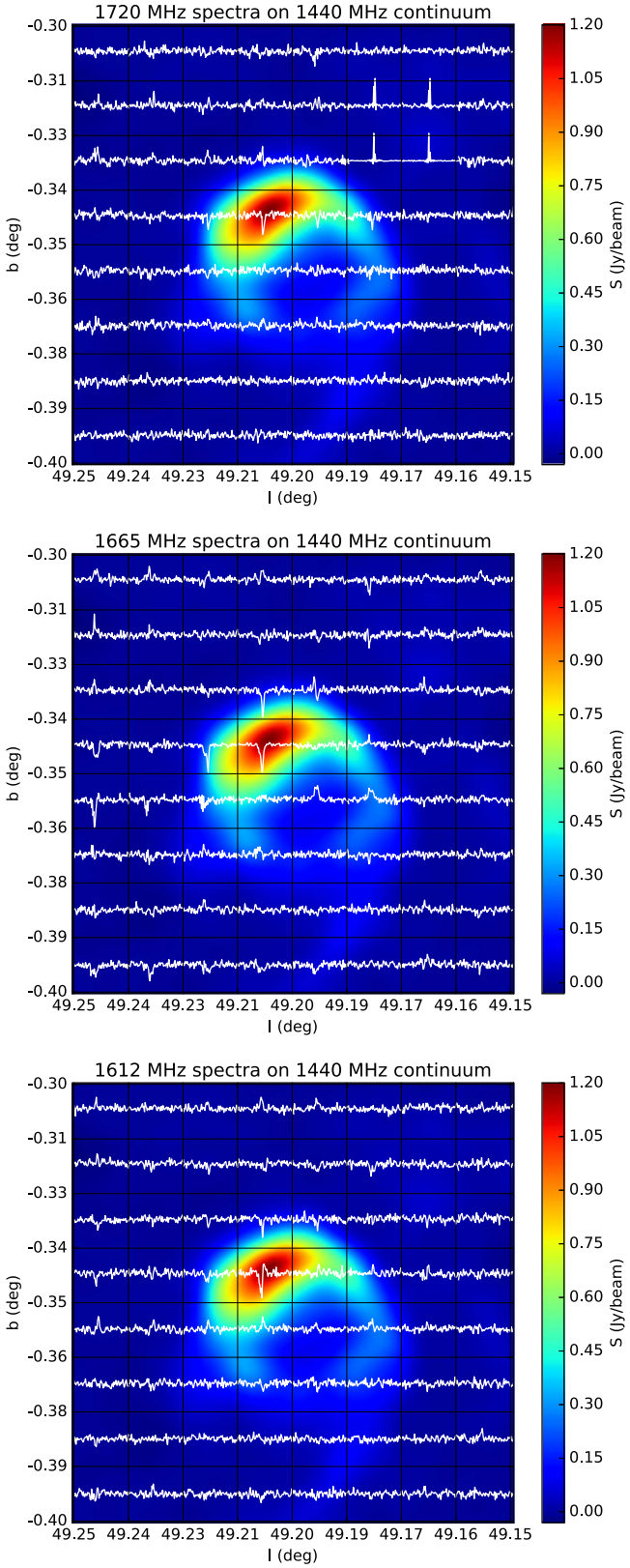

Figure 6. The three figures, respectively, show OH spectral maps of three frequencies (1720/1665/1612 MHz). The background is the 1440 MHz continuum image from *THOR*. The spectrum in every black square shows the mean spectrum from -58.5 km s^{-1} to 135 km s^{-1} in that region. In the first panel, the scale in the region ($49.^{\circ}16 < l < 49.^{\circ}19$, $-0.^{\circ}34 < b < -0.^{\circ}31$) is different from other regions because the 1720 MHz OH maser in the region is so strong that we cannot show it in the same scale. In maser regions, the spectral intensities are divided by 20.

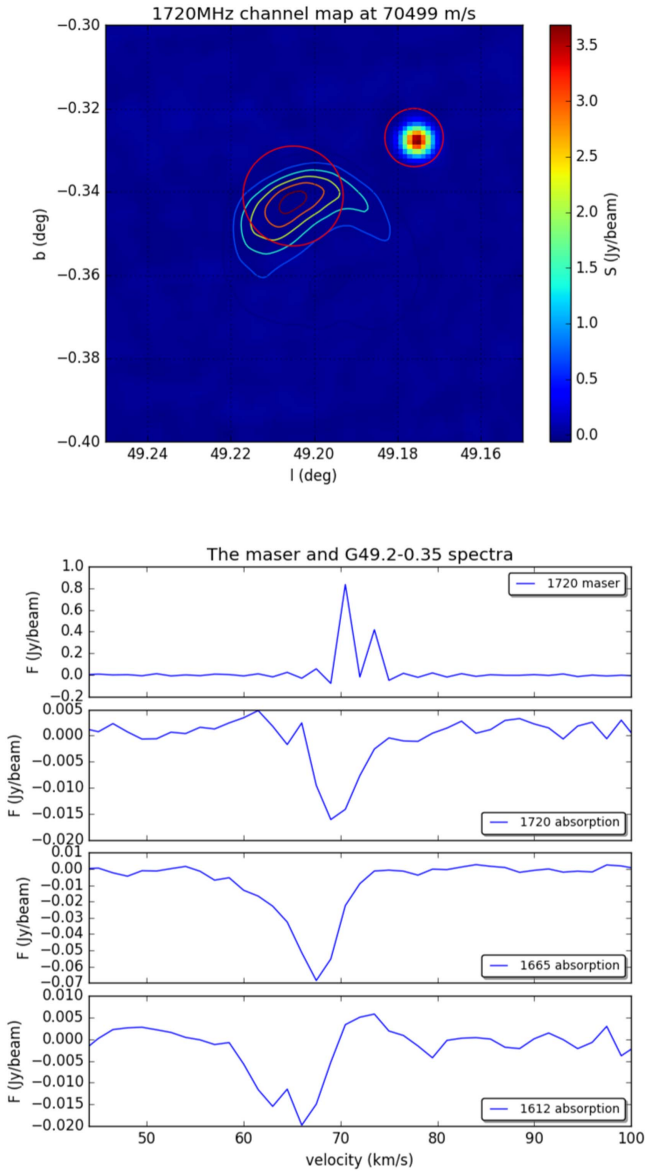

Figure 7. Top panel shows the 1720 MHz channel map toward G49.2-0.35, where the OH maser is very obvious. We plot the contours of the 1440 MHz continuum from *THOR* on the map. The right red circle shows the maser region, while the left red circle shows the absorption region. In the bottom panel, we plot the spectra in the two regions. The first spectrum is the 1720 MHz OH emission at the maser region, and the rest of the spectra are the absorption at the H II region.

we believe the polarization toward the NE region is mainly from W51C. In addition, Velusamy & Kundu (1974) get a total flux density of 51.5 Jy at 11 cm for W51C, so the smallest flux density of the new edge is about 25.7 Jy. Moon & Koo (1994) mentioned strong nonthermal flux density of 28 Jy at 11 cm toward W51A, but they are not sure about its origin. All these clues point to an newly found northeastern SNR edge.

In fact, every SNR explodes approximately spherically, so most of SNRs should have two edges. Even an inhomogeneous ISM is hard to yield a one-edge SNR.

5.2. The Interaction Region

Moon & Koo (1994) estimated a probable nonthermal flux density of 9 Jy at 11 cm toward the H II region G49.2-0.35, which is further supported by Brogan et al. (2013). We also find weak polarized emission toward it in Figure 5. Similar to the new edge, this possibly originates from the SNR. This region is next to the explosion center along the LoS, so this nonthermal emission is possibly from the shell expanding along the LoS. Due to the projection effect, usually a shell expanding along the LoS has low flux density and is difficult to detect. However, such a shell will be detectable if the SNR interacts with an MC (see Figure 2). In fact, we detect the 1720 MHz OH maser in the region, which favors such an SNR–MCs interaction in the region.

In addition, shocks propagating along the LoS will not change the initial direction of the magnetic field toward us. The observed direction of the magnetic field is the same as our assumed initial direction of the magnetic field in the region. Furthermore, the direction of the Galactic large-scale magnetic field around W51 complex is different from the direction in this region. So our assumptions on the origin of the nonthermal emission at this region and the initial direction of magnetic field are self-consistent.

The synthesis of OH molecules is a totally different proceeding from the generation of masers. Shocks dissociate the molecules in MCs and produce OH molecules behind the shock (Wardle 1999). Masers are generated with strict conditions: the temperature, density, and OH column density must be all suitable. Thus most of the OH molecules cannot form masers. These molecules may absorb the continuum emission from the strong background source, such as SNRs and H II regions, then generate absorption lines. Hewitt et al. (2008) believed that detecting a narrow 1720 MHz OH emission line and broadened 1667/1665/1612 MHz absorption lines in the same region are strong evidence of interaction between SNRs and MCs. Such absorption will be rare if the background source is weak. Figure 6 shows that the 1720/1665/1612 MHz absorption is mainly detected in the region with strong background continuum emission. Around the absorption region, there appear to be emissions in the region where the background continuum emission is weak. These features are away from the 1720 MHz OH maser. Since H II regions can also produce OH molecules, these features are likely related to the H II region G49.2-0.35.

Figure 7 reveals that the velocity of the OH absorption features decrease with the frequency of the OH transition. The velocity shift may be very local, rather than being an indicator of galactic kinematic distance, but is not related to the SNR W51C. The fact of detecting the absorptions against the H II region G49.2-0.35 implies that the H II region should lie behind the OH clouds producing the absorption features. Referring to the studies of Brogan et al. (2013) and Ginsburg et al. (2015), G49.2-0.35 lies in front of W51C. If so, the SNR has nothing to do with the OH clouds where these OH absorptions are produced. In fact, there are three masers in the region (Brogan et al. 2013), but the spatial resolution of *THOR* is not enough to distinguish them. Two of the three are close to each other and have almost the same velocity. Thus we can see two lines with peak velocities of 71 and 73 km s^{-1}, respectively, in Figure 7. In addition, 1720 MHz OH masers should be distributed over the SNR, if one SNR shocks the MCs (Wardle & McDonnell 2012). The fact that there are only three masers in the W51B/C region hints that the contact area of SNR shocks and MCs is likely small. A small contact

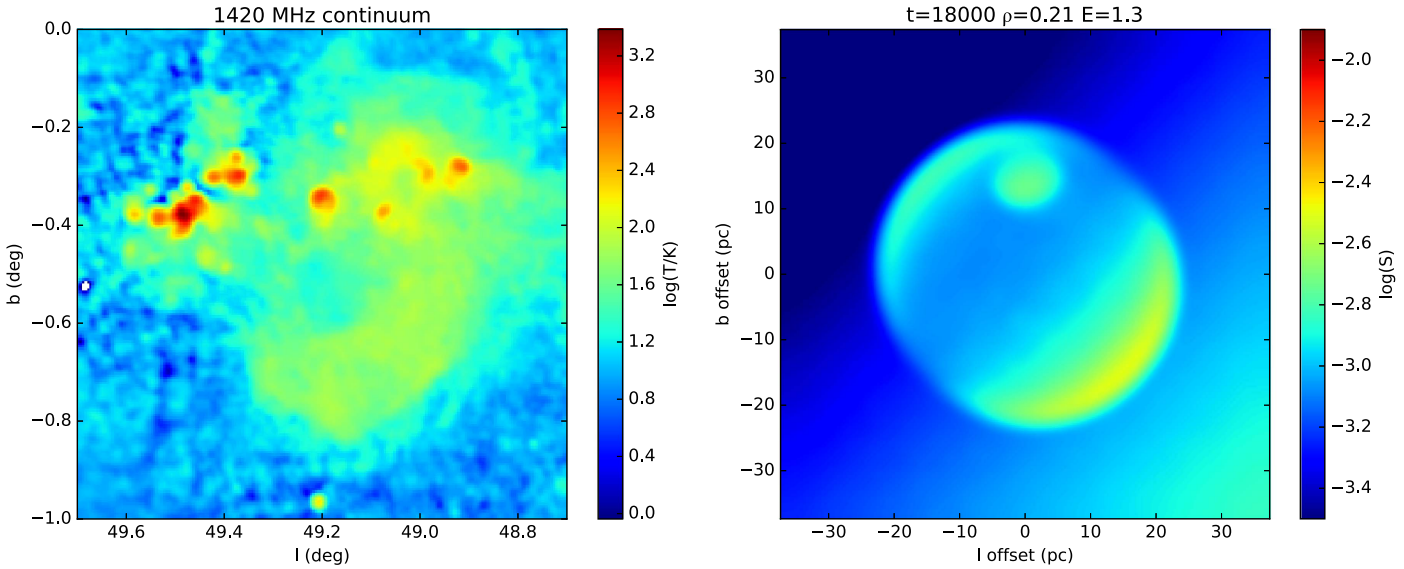

Figure 8. Left panel shows the 1420 MHz continuum map of the W51 complex region. The right panel is the result after changing the color style of the right panel in Figure 2. If we take 4.3 kpc as the distance, the two panels have the same size.

area means a small interaction region, so there are only a few masers.

In conclusion, we suggest that a shock propagating along the LoS, is interacting with an MC. Such a situation is supported by the polarized emission, the nonthermal emission, and OH spectra. It can explain the assumed initial magnetic direction and the few OH masers.

6. Summary

We simulate the evolution of SNR W51C from 850 to 18,000 years. Our simulation reveals a new edge, and that its flux density is higher than the sensitivity of *VGPS*. By analyzing observational data, we find the polarized emission from the new edge, so we conclude that a new edge does exist. In addition, we detect obvious polarized emission in the small H II region G49.2-0.35 next to the explosion center of the simulation, which can be explained as the result of an interaction between SNR shocks and ISM along the LoS. We find the 1612/1665/1720 MHz OH absorption features against H II region G49.2-0.3 and the 1720 MHz OH maser emission spectrum at the W51B/C interface region. We conclude that the absorptions are mostly from the OH gas in front of the H II region G49.2-0.35 and not related to the SNR.

We thank Dr. Reich for explaining the polarization data of Effelsberg. Drs. X. Y. Gao and J. Xu also provided suggestions about polarization data. We thank Drs. Rugel and Beuther for their helpful discussions on *THOR* data. We also thank Dr. J. Fang for his suggestion regarding the supernova remnants simulation. We acknowledge support from the NSFC (11473038,11603039).

ORCID iDs

M. F. Zhang https://orcid.org/0000-0001-8261-3254
W. W. Tian https://orcid.org/0000-0003-3775-3770
D. A. Leahy https://orcid.org/0000-0002-4814-958X

References

Abdo, A. A., Ackermann, M., Ajello, M., et al. 2009, ApJL, 706, L1
Aleksić, J., Alvarez, E. A., Antonelli, L. A., et al. 2012, A&A, 541, A13
Beuther, H., Bihr, S., Rugel, M., et al. 2016, A&A, 595, A32
Brogan, C. L. 2005, in ASP Conf. Ser. 340, Future Directions in High Resolution Astronomy, ed. J. Romney & M. Reid (San Francisco, CA: ASP), 334
Brogan, C. L., Goss, W. M., Hunter, T. R., et al. 2013, ApJ, 771, 91
Copetti, M. V. F., & Schmidt, A. A. 1991, MNRAS, 250, 127
Duncan, A. R., Reich, P., Reich, W., & Fürst, E. 1999, A&A, 350, 447
Genzel, R., Downes, D., Schneps, M. H., et al. 1981, ApJ, 247, 1039
Ginsburg, A., Bally, J., Battersby, C., et al. 2015, A&A, 573, A106
Haverkorn, M. 2015, in Magnetic Fields in Diffuse Media, Astrophysics and Space Science Library, Volume 407, ed. A. Lazarian, E. M. de Gouveia Dal Pino, & C. Melioli (Berlin: Springer), 483
Hewitt, J. W., Yusef-Zadeh, F., & Wardle, M. 2008, ApJ, 683, 189
Junkes, N., Fuerst, E., & Reich, W. 1987, A&AS, 69, 451
Kang, M., Bieging, J. H., Kulesa, C. A., et al. 2010, ApJS, 190, 58
Koo, B.-C., Kim, K.-T., & Seward, F. D. 1995, ApJ, 447, 211
Leahy, D. A. 2017, ApJ, 837, 36
Leahy, D. A., & Williams, J. E. 2017, AJ, 153, 239
Mignone, A., Bodo, G., Massaglia, S., et al. 2007, ApJS, 170, 228
Moon, D.-S., & Koo, B.-C. 1994, JKAS, 27, 81
Orlando, S., Bocchino, F., Reale, F., Peres, G., & Petruk, O. 2007, A&A, 470, 927
Parsons, H., Thompson, M. A., Clark, J. S., & Chrysostomou, A. 2012, MNRAS, 424, 1658
Poznanski, D. 2013, MNRAS, 436, 3224
Sasaki, M., Heinitz, C., Warth, G., & Pühlhofer, G. 2014, A&A, 563, A9
Sato, M., Reid, M. J., Brunthaler, A., & Menten, K. M. 2010, ApJ, 720, 1055
Schneps, M. H., Lane, A. P., Downes, D., et al. 1981, ApJ, 249, 124
Sedov, L. I. 1959, Similarity and Dimensional Methods in Mechanics (New York: Academic)
Shaver, P. A., & Goss, W. M. 1970, AuJPA, 14, 133
Stil, J. M., Taylor, A. R., Dickey, J. M., et al. 2006, AJ, 132, 1158
Subrahmanyan, R., & Goss, W. M. 1995, MNRAS, 275, 755
Sukhbold, T., Ertl, T., Woosley, S. E., Brown, J. M., & Janka, H.-T. 2016, ApJ, 821, 38
Tian, W. W., & Leahy, D. A. 2013, ApJL, 769, L17
Velusamy, T., & Kundu, M. R. 1974, A&A, 32, 375
Wardle, M. 1999, ApJL, 525, L101
Wardle, M., & McDonnell, K. 2012, in IAU Symp. 287, Cosmic Masers—from OH to H0, ed. R. S. Booth, W. H. T. Vlemmings, & E. M. L. Humphreys (Cambridge: Cambridge Univ. Press), 441
Xu, J., & Han, J.-L. 2014, RAA, 14, 942
Xu, Y., Reid, M. J., Menten, K. M., et al. 2009, ApJ, 693, 413